Self-standing cuprous oxide nanoparticles on silica@ polyphosphazene nanospheres: 3D nanostructure for enhancing the flame retardancy and toxic effluents elimination of epoxy resins via synergistic catalytic effect

Shuilai Qiu, Weiyi Xing, Xiaming Feng, Bin Yu, Xiaowei Mu, Richard K. K. Yuen, Yuan Hu

PII: S1385-8947(16)31511-X
DOI: http://dx.doi.org/10.1016/j.cej.2016.10.100
Reference: CEJ 15956

To appear in: *Chemical Engineering Journal*

Received Date: 11 July 2016
Revised Date: 14 October 2016
Accepted Date: 21 October 2016

Please cite this article as: S. Qiu, W. Xing, X. Feng, B. Yu, X. Mu, R. K. K. Yuen, Y. Hu, Self-standing cuprous oxide nanoparticles on silica@ polyphosphazene nanospheres: 3D nanostructure for enhancing the flame retardancy and toxic effluents elimination of epoxy resins via synergistic catalytic effect, *Chemical Engineering Journal* (2016), doi: http://dx.doi.org/10.1016/j.cej.2016.10.100

Self-standing cuprous oxide nanoparticles on silica@ polyphosphazene nanospheres: 3D nanostructure for enhancing the flame retardancy and toxic effluents elimination of epoxy resins via synergistic catalytic effect

Shuilai Qiu [ab], Weiyi Xing [*a], Xiaming Feng [ab], Bin Yu [ab], Xiaowei Mu [a], Richard K. K. Yuen [bc] and Yuan Hu [*ab]

[a] *State Key Laboratory of Fire Science, University of Science and Technology of China, 96 Jinzhai Road, Hefei, Anhui 230026, P.R. China*

[b] *USTC-CityU Joint Advanced Research Centre, Suzhou Key Laboratory of Urban Public Safety, Suzhou Institute for Advanced Study, University of Science and Technology of China, 166 Ren'ai Road, Suzhou, Jiangsu 215123, P. R. China*

[c] *Department of Architecture and Civil Engineering, City University of Hong Kong, Tat Chee Avenue, Kowloon, Hong Kong*

Abstract: A novel strategy was developed for the preparation of 3D nanostructure to improve the flame retardancy and toxic effluents elimination of epoxy resins (EP) via synergistic catalytic effect. Herein, the synthesis of cross-linked organic–inorganic polyphosphazene nanoshells (PZM) with amino-rich groups was reported via a facile condensation polymerization of hexachlorocyclotriphosphazene (HCCP) and 4,4′-diaminodiphenyl ether (ODA) on silica (SiO_2) nanospheres as templates. Then cuprous oxide nanoparticles (Cu_2O NPs) were synthesized by simultaneous chemical reduction method on the surface of polyphosphazene nanoshells. Subsequently, the obtained SiO_2@PZM@Cu spheres were incorporated into the EP to prepare samples for investigation of their flame-retardant and toxicity suppression performance. Herein, cone results indicated that the incorporation of 2 wt% SiO_2@PZM@Cu obviously improved the flame-retardant performance of EP, such as 37.9% reduction in peak heat release rate and 31.3% decrease in total heat release. On the other hand, the amount of toxic CO and other volatile gas products from the EP decomposition significantly suppressed after incorporating the SiO_2@PZM@Cu, implying a reduced toxicity. In addition, a mechanism for the flame retardancy and toxicity elimination was proposed. It is reasonable to believe that the enhanced flame retardancy and toxic effluents elimination for nanocomposites are attributed to synergistic effect from respective components (Cu_2O NPs and PZM) plus the SiO_2 spheres.

Keywords: SiO_2@PZM@Cu, nanocomposites, flame retardant, toxic effluents elimination, mechanism

1. Introduction

Polyphosphazenes are a family of versatile hybrid organic–inorganic materials that they have numerous outstanding properties. The presence of the phosphazene unit (–P=N–) in the backbone and structural multiplicity of side groups, provides vast flexibility to functionalize the materials through physical and/or chemical modifications [1,2]. Therefore, it is well known that polyphosphazenes have a flexible range of applications such as biomaterials, optical materials, electrical materials, membrane materials, and hybrid materials, etc., because of their outstanding high thermal stability and structural diversity [3,4]. As expected, polyphosphazenes are attractive candidates as flame-retardant additives, which can be divided into three types of polymers, like, linear polyphosphazenes and the polymers with cyclophosphazene units in backbone or side chain [5,6]. All these polymer materials exhibit high limiting oxygen index (LOI) values and enhance the flame retardancy of polymer matrices significantly. In addition to these merits, the linear polyphosphazenes have the main disadvantages, such as low output and high cost is restricting their application [7,8]. But, the other type of polyphosphazenes that have attracted attention are cyclotriphosphazenes, which possess a backbone of –P=N– unit, exhibit good flame retardancy and self-extinction [9,10]. Cyclotriphosphazenes have been used to fabricate nano- and microscale polymers by condensation polymerization, such as polyphosphazene nanotubes, microspheres, nanochain and nanofibers [11-13]. These synthesized nanomaterials may endow high thermal stability, flame retardancy and radiation resistance [14]. In this decade, a series of polyphosphazene nanomaterials have been reported and used as enhancing additives, crosslinking agent and flame-retardant polymeric additives [15-16]. But, interestingly up to now, there is rare report about the flame retardancy of polyphosphazene nanomaterials in polymer matrices [17], and how to combine these nanomaterials with other flame retardants to further improve flame retardant efficiency.

On the other hand, metal oxide catalysts have been applied to eliminate the toxic gasses, such as hydrocarbons, CO, NO_x, and HCN, *etc.* [18,19], from polymeric

combustion, and they can be expecting for partly catalytic oxidation into harmless gasses, such as H_2O, CO_2, and N_2, *etc*. Therefore, metal oxides are playing an important role as nanoadditives in polymer nanocomposites with different surface morphological features and higher thermal stability [20,21]. Among them, cuprous oxide (Cu_2O), as a p-type semiconductor with a direct band gap (Eg = 2.17 eV) was widely utilized, because it is non-toxic, relatively cheap and widely abundant, and has been also used as heterogeneous catalysts, gas sensors and nanodiscs for battery electrodes [22,23]. Moreover, Cu_2O NPs are incorporated into the polymeric matrix that leads to enhanced thermal stability and thermal conductivity of the nanocomposites [24,25]. In this connection various oxidation activities of CO over different valences of copper oxides, like Cu, Cu_2O, and CuO have been investigated by Huang *et al.*, and reported that the Cu_2O have been exhibited higher activity than the other two copper species may due to its ability to capture or release surface lattice oxygen more easily [26]. White et al prepared nearly monodisperse Cu_2O NPs by the thermal decomposition of a Cu precursor, and which was exhibited exceptional CO oxidation activities in $CO/N_2/O_2$ mixture over 99.5% conversion of CO to CO_2 achieved [27]. In the previous studies, metal oxides were used as flame retardant synergists and toxic gas suppressants for polymer materials. It has been reported that the metal oxides, such as CuO, Co_3O_4, MnO_2, and SnO_2, etc., are combined with graphene to improve the flame retardancy of polymers via promoting the char formation [28-30]. Therefore, Cu_2O has been utilized in decreasing the total smoke emission and toxic CO of polymers due to its catalytic reductive-coupling and charring effect in the condensed phase [31]. In this connection we have an idea of "can metal oxide, especially Cu_2O, have synergistic catalytic effect with polyphosphazenes on the oxidation of CO to CO_2 at the smoke-rich environment?

On the third hand, epoxy resin (EP) is a commonly used thermosetting material, which has an extensive range of applications at adhesive, potting, laminating and coating areas, due to its dimensional stability and excellent mechanical performance [32-34]. However, the limitations of its high flammability and release of large amount of smoke and toxic gases during combustion restrict its application in many fields. To

solve these problems, many strategies have been utilizing to enhance the flame retardancy of EP. In this connection, incorporation of nanoadditives, such as MoS_2 [35], graphene [36,37], boron nitride [38], layered double hydroxide [39], carbon nanotubes [40], and nanosilica [41], is one of the methods which can improve the integrate performance of EP. Qian *et al.* [42] investigated the fire safety and mechanical properties of FRs-rGO/EP nanocomposites, with the incorporation of 5 wt% of FRs-rGO into EP, satisfied flame retardant grade (V0) and the LOI as high as 29.5 were achieved. Moreover, the peak heat release rate (PHRR) value of FRs-rGO/EP was significantly reduced by 35%. Jiang *et al.* [43] prepared another mesoporous silica@Co−Al layered double hydroxide (m-SiO_2@Co−Al LDH) spheres, significant decreases in the PHRR of 39.3% and THR of 36.2% were achieved with the addition of 2 wt% m-SiO_2@Co−Al LDH into EP, respectively. Therefore, in summary (Table 1), the combustion properties of EP by incorporation of various kinds of nano-additives have been achieved good improvements in their flame retardancy, thermal and/or mechanical properties. In addition to this, for the better and efficient improvement in the flame retardancy by reducing the smoke toxicity of EP, polyphosphazene and Cu_2O are chosen to constitute a synergistic flame retardant system. Furthermore, it has been reported that the silica (SiO_2) as an efficient solid acid for catalytic degradation of the polymer, and could be easily catalyzed carbonization of the degradation products in the presence of metal oxides follows [49].

In view of the above observations and our new idea of CO to CO_2 at the smoke-rich environment by synergistic catalytic effect of Cu_2O with polyphosphazenes, herein, we developed a facile procedure for preparation of a new three-dimensional (3D) organic−inorganic core-shell nanostructures by growing poly-(cyclotriphospazene-co-4,4′-diaminodiphenyl ether) (PZM) on the surface of silica (SiO_2) nanospheres and used as accurate templates. These newly developed core-shell nanostructures possess good stabilizing abilities and provide anchoring sites for the formation of Cu_2O NPs. Subsequently, SiO_2@PZM@Cu was obtained by loading the Cu_2O NPs on the SiO_2@PZM core-shell structure via chemical reduction

(Scheme 1). SiO_2@PZM@Cu hybrids were then added into the EP matrix for investigating their flame retardancy and toxic effluents elimination during the combustion. It is anticipated that the combination of SiO_2, PZM and Cu_2O could effectively enhance the flame retardant property and reduce toxic effluents during the combustion of EP.

2. Experimental section

2.1. Materials

Hexachlorocyclotriphosphazene (HCCP), 4,4′-diaminodiphenyl ether (ODA) and 4,4′-diaminodiphenylmethane (DDM) were purchased from Aldrich Chemical Co. Ltd. (U.S.). Anhydrous ethanol, ammonium hydroxide ($NH_3 \cdot H_2O$), hydrazine hydrate (85%), tetraethyl orthosilicate (TEOS), triethylamine (TEA), tetrahydrofuran (THF), acetonitrile, acetone, cupric acetate monohydrate and poly(N-vinylpyrrolidone) (PVP) were obtained from Sinopharm Chemical Reagent Co., Ltd. (China). EP (DGEBA, E-44) was supplied by Hefei Jiangfeng Chemical Industry Co. Ltd. (China). Tetrahydrofuran (THF), acetonitrile and triethylamine (TEA) were dried over 4 ° A molecular sieves before use.

2.2. Preparation of SiO_2 nanospheres

SiO_2 nanospheres were prepared according to the previous method with slight modification [50]. In a typical procedure, $NH_3 \cdot H_2O$ (100 mL) was mixed with anhydrous ethanol (300 mL) to obtain solution A. On the aside TEOS (1 mL) was mixed with anhydrous ethanol (9 mL) to obtain solution B. Then the solution B was slowly added dropwise to solution A while stirring uniformly. The resulting mixture was stirred at room temperature until the solution became muddy. White colloidal particles were collected by centrifugation at 8500 rpm for 5 min, washed with ethanol (20 mL × 3), dried and finally dispersed in acetonitrile (30 mg/mL) as a stock solution.

2.3. Preparation of SiO_2@PZM nanospheres

SiO_2 nanospheres were dispersed in acetonitrile (0.2 mg/mL, 50 mL) by ultrasonication. ODA (40 mg) and TEA (3 mL) were then added to the suspension,

respectively. Then the solution of HCCP (20 mg) in 5 mL of acetonitrile was added dropwise to the system within 30 min. The mixture was controlled at 40 °C with ultrasonication (53 kHz) for an additional 6 h. After completion of the reaction, the resulting SiO_2@PZM were collected by centrifugation at 8500 rpm for 5 min and washed with ethanol (20 mL × 3), and then dried under vacuum at 60 °C.

2.4. Preparation of SiO_2@PZM@Cu nanospheres by the reduction process

The chemical reduction of copper acetate by hydrazine hydrate was conducted to generate Cu_2O on the SiO_2@PZM. Briefly, 0.2 g of SiO_2@PZM was dispersed in aqueous solution of copper acetate (1.2 mM, 200 mL) with the assistance of ultrasonication at room temperature. Then, PVP (0.05 mM) was added to above solution, and the pH of the reaction solution was adjusted to 9-11 with ammonia solution. The reaction mixture was heated to 50 °C and stirred for 2 h. Finally, the aqueous solution of hydrazine hydrate (0.3 M, 20mL) was dropped slowly into the reaction system within 15 min. The resulting mixture was stirred at 70 °C for 1h, giving a red colloid. The SiO_2@PZM@Cu hybrids were obtained and dried at 40 °C.

2.5. Preparation of EP/SiO_2@PZM@Cu composite

A typical preparation of epoxy composite containing 2 wt% SiO_2@PZM@Cu is illustrated below: A quantity of 0.9 g of SiO_2@PZM@Cu (2.0 wt%) was dispersed in 30 mL of acetone solution by ultrasonic treatment for 30 min. Then, 36.2 g of EP was added to the above solution with mechanical stirring for 2 h. The solvent was removed in a vacuum oven at 60 °C for 6 h. Subsequently, 7.9 g of DDM was melt and mixed with the above mixture by a vigorous stirring for 1 min. Finally, the sample named as EP/SiO_2@PZM@Cu2 was cured at 100 and 150 °C for 2 h, respectively. After curing, the sample was permitted to cool to room temperature. For the preparation of pure EP, EP/SiO_2 (1.0 wt%), EP/SiO_2@PZM (1.0 wt%) and EP/SiO_2@PZM@Cu1 (1.0 wt%) composites, a similar procedure was adopted except the type of the nanoadditives.

2.6. Characterization

Fourier transform infrared (FTIR) spectra were obtained on a Nicolet 6700 spectrometer (Nicolet Instrument Co., USA). X-ray diffraction (XRD) patterns were

recorded on an X-ray diffractometer (Rigaku Co., Japan), using Cu K_α radiation (λ= 0.15418 nm), at a scanning rate of 4 ° min^{-1}. X-Ray photoelectron spectroscopy (XPS) test was performed with a VG ESCALAB MK-II electron spectrometer (V.G. Scientific Ltd., UK) employing a monochromatic Al K α X-ray source. Transmission electron microscopy (TEM) and energy dispersive X-ray spectroscopy (EDX) were carried out using a JEM-2100F transmission electron microscopy (Japan Electron Optics Laboratory Co., Ltd., Japan). Before measurement, samples were dispersed in ethanol with ultrasonication for 30 min, and then dripped onto copper grids for observation. Thermogravimetric analysis (TGA) was performed on a Q5000 thermo-analyzer instrument (TA Instruments Inc., USA) from 20 to 800 ^oC at a linear heating rate of 20 ^oC min^{-1} under nitrogen atmospheres. The combustion properties of EP and its composites were conducted on a cone calorimeter based on ASTM E1354/ISO 5660. Every specimen with the sizes of 100 × 100 × 3 mm^3 was exposed horizontally to a heat flux of 35 kW/m^2. Microstructures of the char residues and fracture surface of the EP composites were conducted by high-resolution JEOL JSM-6700 field-emission scanning electron microscopy (FE-SEM). The structure and components of the char residue of EP composites were investigated by an LABRAM-HR laser confocal microRaman spectrometer (Jobin Yvon Co., Ltd., France) with an argon laser of 514.5 nm. Thermogravimetric analysis/infrared spectrometry (TG-IR) was performed using a TGA Q5000 thermogravimetric analyzer, which was coupled with a Nicolet 6700 FT-IR spectrophotometer through a stainless steel transfer pipe.

3. Results and discussion

3.1. Synthesis and characterization of SiO_2@PZM@Cu nanospheres

The preparation of SiO_2@PZM@Cu nanospheres is a straightforward strategy based on a one-pot synthesis of cross-linked PZM nanoshells on silica nanospheres which as accurate templates (Scheme 1). Firstly, the PZM nanoshells were formed by cross-linked precipitation polymerization using HCCP and ODA as co-monomers and spontaneously attach onto the surface of SiO_2 due to the low surface energy of PZM.

Furtherly, the cross-linking polymerization among the PZM nanoparticles was then conducted sequentially, resulting in the generation of shells on the surface of SiO_2 nanospheres. Secondly, the resulting SiO_2@PZM nanospheres have been utilized for Cu_2O NPs decoration after purification. Herein, the active amino groups of PZM nanoshells which give SiO_2@PZM nanospheres with hydrophilic nature and anchoring sites for the loading of Cu_2O NPs. Homogeneous dispersion of Cu_2O NPs on the surface of SiO_2@PZM resulted in the 3D nanostructure named as SiO_2@PZM@Cu.

To examine the successful formation of SiO_2 spheres with given size, surface morphology was investigated by the TEM (Fig. 1A) and SEM (Fig. 1D). Neat SiO_2 spheres have relatively smooth outer surface morphology with controllable size, have an average diameter of ca. 350±15 nm. It can be obvious seen that all of the SiO_2 spheres exhibit high monodispersity and spherical morphology, and which is suitable for using as a template material to conduct further treatment. SiO_2 template with rich hydroxyl groups provides attaches sites for cross-linking polymerization to form polyphosphazene nanoshells. For SiO_2@PZM nanospheres (Fig. 1B and C), the spherical morphology is preserved after the silica templates were wrapping by the polyphosphazene phase, and core-shell structure of SiO_2@PZM particle is clearly observed due to the electronic contrast of PZM shell to SiO_2 core. The conspicuous difference is that the relative roughness surface of polyphosphazene shell. Fig. 1B shows that the SiO_2@PZM nanospheres are monodispersed with a diameter of 580±10 nm, a bit bigger than that of neat SiO_2 spheres observed from SEM image (Fig. 1D, E); As can be seen from the SEM image that several smaller nanoparticles with a diameter of about 100 nm are observed, which is due to the self-polymerization of HCCP and ODA to form PZM nanospheres without core.

Fig. 2 presents representative TEM images (A, B and C) and SEM images (D and E) of the SiO_2@PZM@Cu at different magnifications. The Cu_2O NPs are observed as dark spots on the surfaces of the SiO_2@PZM nanospheres. Most Cu_2O NPs distribute homogeneously on the SiO_2@PZM surfaces, and a part aggregates consisting of several nanoparticles are observed. Digital analysis on representative

TEM image (100 nanoparticles measured) yielded an average Cu_2O NP size of 18–25 nm. Based on the TEM images above, it can be seen that the nature of SiO_2@PZM scaffold plays an important role during the formation of the Cu_2O NPs with uniform size and good dispersibility. As we have obtained, the surface of SiO_2@PZM@Cu nanospheres loads several self-standing Cu_2O NPs. The presence of Cu_2O NPs and PZM shells and their coating on the surface of SiO_2 core have been confirmed using EDX, shown in Fig. 2F.

FT-IR spectra were employed to confirm the occurrence of polycondensation reaction between the co-monomers HCCP and ODA. As shown in Fig. 3A, the typical peaks of the SiO_2 spectrum at 1105 and 800 cm^{-1} corresponding to Si-O-Si stretching and bending vibrations [44]; the absorption peak at 953 cm^{-1} is attributed to Si-OH stretching vibration. After coating with polyphosphazene and loading with Cu_2O NPs, three apparent peaks at 1604, 1500 and 1456 cm^{-1} are assigned to the stretching vibration of the C=C group in the phenylene of ODA units. The strong peaks at 1198 and 849 cm^{-1} are associated with the P=N and P–N characteristic absorption of the cyclotriphosphazene, respectively. The sharp peaks at 1198 and 1100 cm^{-1} are attributed to the stretching vibration of the ether bond, and the absorption peak at 3370 cm^{-1} corresponds to the amino in ODA units, are both observed in the spectra of SiO_2@PZM and SiO_2@PZM@Cu.

The existence of elemental Cu can be determined by EDX characterization in the TEM test. The XRD pattern for the SiO_2@PZM@Cu further confirmed the above results. Fig. 3B exhibits the XRD patterns of neat SiO_2, SiO_2@PZM and SiO_2@PZM@Cu. The diffraction pattern of SiO_2 depicts a reflection characteristic of amorphous silica [51]. After coating with the PZM nanoshells, a broad peak is ascribed to the amorphous PZM matrix, can be observed beside silica. The XRD pattern of SiO_2@PZM@Cu confirms that the nanoparticles procured on the PZM substrate are Cu_2O, the characteristic peaks attributing to face-centered-cubic structure of Cu_2O NPs are observe, which means nanoparticles are in the same crystalline structure as bulk Cu. It also presents peaks corresponding to copper nanocrystals (Cu), which confirms certain degree of over-reduction in sample which

might have taken place during sample transfer or sample preparation.

XPS offers plentiful information about surface composition and chemical state of SiO_2 and SiO_2@PZM and SiO_2@PZM@Cu. The XPS survey spectrum of SiO_2@PZM@Cu (Fig. 3C) shows that the sample includes Si, O, C, P, N and Cu elements, implying the formation of SiO_2@PZM@Cu. The surface of SiO_2@PZM nanosphere is composed of C, O, P and N elements; meanwhile, the N and P atoms percentage is 11.7% and 3.5%, respectively. The mole ratio of N:P is in accordance with the theoretical value for polyphosphazene shells with highly cross-linked chemical structure. The Cu 2p spectrum is deconvoluted into Cu $2p_{3/2}$ and Cu $2p_{1/2}$ located at 934.2 and 954.0 eV. The XPS Cu 2p spectra indicate that copper existing different state. Combined with the results of TEM, SEM, EDX, FT-IR, XRD and XPS, it is reasonable to demonstrate that the 3D nanostructure included SiO_2, PZM and Cu_2O NPs was successfully synthesized.

3.2. Thermal stability of EP and its nanocomposites.

The thermal stability of SiO_2, SiO_2@PZM and SiO_2@PZM@Cu was evaluated by TGA in nitrogen atmosphere. The temperatures at which 5% and maximum mass loss occurs are defined as the initial degradation temperature ($T_{-5\%}$) and maximum degradation temperature (T_{max}), respectively. As can be observed in Fig. 3D, neat SiO_2 shows a three-step weight loss. The first stage is attributed to the loss of physically adsorbed water, while the second is assigned to the degradation of the silica network. SiO_2@PZM also exhibits a three-step mass loss profile accompanied a residual char of about 79.4%, the early two stage degradation as the same as pure SiO_2. The third stage should be attributing to polyphosphazene substrate (490-579 °C). In comparison, SiO_2@PZM@Cu presents a continuous mass loss with a residual char of about 88.4%, indicating that the integration of SiO_2, PZM with Cu_2O NPs obviously enhances the thermal stability of the hybrid materials.

From Fig. 4 and Table 2, EP/SiO_2@PZM@Cu nanocomposites are less thermally stable than pure EP when evaluated by $T_{-5\%}$ and $T_{-50\%}$, which is possibly ascribed to the catalysis degradation initiated by Cu_2O NPs attached on PZM surfaces. At higher temperatures, the EP molecular chains connected by the amino-rich SiO_2@PZM walls

as cross-linking network shows high thermal stability due to the barrier effect of its network structure, leading to a delayed degradation process of EP. It is well known that transition metals including copper resulting in catalytic degradation of polymer [52]. As expected, the incorporation of Cu_2O NPs results in an earlier degradation process of EP. Also, the introduction of SiO_2@PZM@Cu leads to the decrease of maximum degradation temperature, which is attributing to the earlier degradation of EP matrix triggered by the catalytic action of Cu_2O NPs. However, compared to EP/SiO_2 and EP/SiO_2@PZM, EP/SiO_2@PZM@Cu nanocomposite presents the improved thermal stability. As far as the char yield is concerned, the incorporation of SiO_2@PZM@Cu results in the improvement of the char residues at 800 °C, due to the catalytic carbonization effect of Cu_2O NPs. Furthermore, from the DTG profiles, the maximum mass loss rates (the peak of DTG curve) of EP/SiO_2@PZM and EP/SiO_2@PZM@Cu composites are lower than that of pure EP, indicating that PZM plays an effective mass-transport barrier role.

To understand the compatibility between SiO_2@PZM@Cu and EP matrix, the freeze-fractured surface microstructures of EP nanocomposites were investigated by FE-SEM. The fracture roughness of polymer nanocomposites reflects the dispersion level and interfacial interaction. It can be clearly seen from Fig. 5A that the pure EP shows a smooth fracture surface. The fracture surfaces of EP/SiO_2 (Fig. 5B) and EP/SiO_2@PZM (Fig. 5C) are much rougher than that of pure EP. Several pulled-out SiO_2@PZM nanoparticles and obvious “scratch” can be observed from Fig. 5C, which can result in the strong interfacial interaction between nanofillers and polymer matrix. It is clear that the fracture surface roughness of the EP/SiO_2@PZM@Cu nanocomposites (Fig. 5D, 5E and 5F) increase with increasing addition of SiO_2@PZM@Cu. In addition, it is observed that numerous SiO_2@PZM@Cu nanospheres are embedded on the fracture surface of EP matrix uniformly. Nevertheless, few nanoparticles agglomerates emerge in the SEM image of EP/SiO_2@PZM@Cu2 sample (Fig. 5F).

3.3. Fire properties of EP and its composites.

Cone calorimeter is a widely used tool for evaluating combustion behaviors of

various materials under real-world fire condition. Heat release rate (HRR) and Total heat release (THR) curves for EP and its nanocomposites are displayed in Fig. 6, and several important parameters obtained from cone calorimeter are listed in Table 3, such as the time to peak heat release rate (T_{PHRR}), PHRR, THR, the peak smoke production rate (PSPR), the total smoke release (TSR), and maximum average heat rate emission (MAHRE) values. Compared to pure EP, the incorporation of 2 wt% SiO_2@PZM@Cu brings about a 37.9% maximum decrease in PHRR, a 31.3% maximum decrease in THR, a 47.9% maximum decrease in PSPR, a 41.9% maximum decrease in TSR, and a 28.1% maximum decrease in MAHRE. The smoke production rate (SPR) and TSR curves of EP and its composites are shown in Fig. 7. Pure EP releases large amount of smoke with high values of PSPR and TSR, due to its multi-aromatic structures. SiO_2 and PZM exhibit slight decrease in the PSPR. The incorporation of SiO_2@PZM@Cu results in the further reduction in PSPR. Fig. 7B reveals that the TSR values of EP composites show a similar trend to that of the PSPR. EP/SiO_2@PZM@Cu2 exhibits a lower TSR value than all samples. The TSR values of the EP nanocomposites are reduced upon increasing the loading of SiO_2@PZM@Cu. The above results reveal that the EP/SiO_2@PZM@Cu2 nanocomposite exhibits the best flame retardancy among all the composites, which indicated the denser protective char layers acts as physic barriers constitutes by the cooperation of SiO_2 nanospheres, polyphosphazene nanoshells and Cu_2O NPs in EP/SiO_2@PZM@Cu composites are more effective than the layers formed by silica in EP/SiO_2 and SiO_2@PZM core-shell structure in EP/SiO_2@PZM.

3.4. Gas and condensed phase analysis

To further investigate the toxic effluents capture and elimination behavior of SiO_2@PZM@Cu, the toxic gases released from EP, EP/SiO_2, EP/SiO_2@PZM and EP/SiO_2@PZM@Cu1 (1 wt%) decomposition were detected by using a TG-FTIR technique. 3D TG-FTIR and FTIR spectra which obtained at the maximum evolution rate during the thermal decomposition of EP nanocomposites are shown in Fig. 8. Several toxic gaseous products are remarkably identified by characteristic strong FTIR peaks. The characteristic signals of the pyrolysis gaseous products appear in the

regions of 3500–4000 cm^{-1}, 2750–3200 cm^{-1}, 2200–2400 cm^{-1}, 1750–1900 cm^{-1}, 1250–1600 cm^{-1} and 600–1000 cm^{-1}. Some toxic gaseous products are weaker identified by characteristic strong FTIR signals, after incorporated SiO_2@PZM@Cu. FTIR spectra of the pyrolysis products for (A) EP and (B) EP/SiO_2@PZM@Cu1 at different temperatures are shown in Fig. 9. The FTIR spectra of EP/SiO_2@PZM@Cu1 are similar to that of EP. The peak at 3650 cm^{-1} is assigned to the vibration of O-H; the peak at 2930 cm^{-1} is attributed to the stretching vibration of CH_2 or CH_3 groups in hydrocarbons; the peaks at 2360 and 2190 cm^{-1} corresponds to the absorption of CO_2 and CO, respectively. Moreover, the peaks at 1740 and 1510 cm^{-1} are attributed to the characteristic bands of carbonyl compounds and aromatic rings, respectively. However, the EP/SiO_2@PZM@Cu1 sample starts to release the pyrolysis products slightly earlier than pure EP, indicating that incorporation of SiO_2@PZM@Cu catalyzes the thermal degradation of EP.

In order to make a comparison, the intensities of total pyrolysis volatiles and representative pyrolysis products for EP nanocomposites are presented in Fig. 10. With the incorporation of SiO_2@PZM@Cu, the maximum absorbance intensity of toxic gases emission is shifted to lowest value, containing total release, hydrocarbons, CO, CO_2, carbonyl and aromatic compounds, compared to that of pure EP, EP/SiO_2 and EP/SiO_2@PZM samples. The decreased intensity of pyrolysis products is attributed to more compact and cohesive char layer as reinforced physical barrier, which retards the escape of volatile degradation products. The major source of smoke particles, from the organic volatiles such as hydrocarbons, carbonyl and aromatic compounds, and the decrease in these volatiles leads to the smoke suppression. Moreover, the CO decrease gives rise to the reduction in smoke toxicity during the combustion, which is beneficial for the improvement of fire safety.

To understand the flame-retardant mechanism, the char residues of EP and its nanocomposites from cone calorimeter test were investigated. During the combustion, neat EP is completely melted to warping and burn dramatically, a part of char residue left after the test, as shown in Fig. 11A. The incorporation of EP/SiO_2@PZM@Cu1 leads to the remarkable improvement of the char yield (Figure 11B), corresponding to

the TGA results. Raman spectroscopy was utilized to characterize the structure and component of the char residues. The Raman spectra of the residues of EP and EP/SiO_2@PZM@Cu1 (Fig. 11C, D) depict two bands at 1596 cm^{-1} and 1365 cm^{-1}, which are named G and D peak, respectively [53]. The area ratio of D to G band (I_D/I_G) is used to evaluate the graphitization degree of the char residue; relative lower I_D/I_G value indicates higher graphitization degree of the char [54]. The value of I_D/I_G for neat EP is 2.83, whereas the EP/SiO_2@PZM@Cu1 exhibits lower value (2.71), suggesting the higher graphitization degree. The present results indicate the formation of the graphitized char during EP composites combustion, due to the synergistic catalytic effect of polyphosphazenes and Cu_2O NPs. It is well-known that the graphitized char is more effective to suppress the heat and mass transfer during combustion than glassy carbon or disordered graphite, which is attributed to its higher compactness and thermal stability. Furthermore, Fig. 11E and F show the SEM images of the external char residues for EP and EP/SiO_2@PZM@Cu1. It is obviously observed that a continuous and compact char surface is formed after the EP/SiO_2@PZM@Cu1 combustion. The char surface with a more cohesive and compact layer is beneficial to the inhibition of heat and mass transfer, thereby enhancing the flame retardancy.

Fig. 12 presents (A) FTIR spectra and (B) XRD patterns of the char residues for EP, EP/SiO_2, EP/SiO_2@PZM and EP/SiO_2@PZM@Cu1 after cone calorimeter tests. As shown in FTIR spectra, the peaks at 1585 and 735 cm^{-1} is attributed to multi-aromatic structure. Pure EP and its composites show the similar char structure, whereas a sharp new peak at approximately 1110 and 806 cm^{-1} corresponding to Si-O-Si stretching and bending vibrations, indicating the remaining silica in the char residues of the EP nanocomposites. For the char residues of EP/SiO_2@PZM and EP/SiO_2@PZM@Cu, a weak absorption peak at 880 cm^{-1} is observed, correspond to P–N characteristic absorption of cyclotriphosphazene, implying the formation of crosslinked phosphorus oxynitride [55]. The XRD pattern of pure EP reveals a broad diffraction peak at approximately 23°, which is attributed to (002) diffraction of graphite. The XRD patterns of EP/SiO_2 and EP/SiO_2@PZM are similar to that of pure

EP, indicating the formation of graphitized carbon. In the XRD pattern of EP/SiO_2@PZM@Cu (1 wt%), several reflections of monoclinic copper oxide (CuO) phase are clearly observed [56], which indicate that most Cu_2O are finally oxidized to CuO during burning of EP/SiO_2@PZM@Cu1, in accordance with the mechanism proposed in scheme 2. Hence, the CuO, multi-aromatic carbon, crosslinked phosphorus oxynitride and SiO_2 on the surface of char layer for EP/SiO_2@PZM@Cu1 exhibits high thermal stability, and act as an effective barrier to inhibit mass and heat transfer between gas phase and condensed phase.

3.5. Flame retardant and toxic effluents elimination mechanism

Based on the analysis of char residues and pyrolysis products, the mechanism is proposed for the flame retardancy and reduced toxicity of EP/SiO_2@PZM@Cu, as shown in scheme 2. On one hand, the metal catalysis has been reported to be an effective method to reduce toxic products during combustion [57]. As an important functional metal element, Cu species have outstanding catalytic effects due to their distinctive physical and chemical properties. In copper oxides, Cu_2O is commonly considered to be more active for CO oxidation [26,58]. Cu_2O plays a role in conversion of CO to CO_2 through a redox cycle, including the oxidation of Cu^+–Cu^{2+} by O_2 and the reduction of Cu^+–Cu^0 by CO [59,60]. Moreover, the presence of SiO_2 can enhance the catalytic ability of Cu_2O. Actually, prior literatures reported that SiO_2 acts as an efficient solid acid for catalytic degradation of polymer due to the presence of many acid sites, and the degradation products could be easily catalyzed carbonization in the presence of metal oxides [49]. Therefore, it is reasonably believed that the combination of catalytic effect for Cu_2O and SiO_2 plays a key role in the elimination of toxic gases and enhancing flame retardancy. On the other hand, for PZM, on the basis of the formation of carbonized aromatic networks and crosslinked phosphorus oxynitride during combustion into account [55], we propose an intumescent flame-retardant mechanism for the polyphosphazenes polymers, due to the EP/SiO_2@PZM@Cu1 can swell into a foam-like structure with a continuous and compact surface when exposed to fire, as shown in Fig. 11B. Meanwhile, phosphorus elements act as a role in the condensed phase to promote char formation. Overall, it is

reasonable to believe that the enhanced flame retardant property and toxic effluents elimination for EP/SiO_2@PZM@Cu is attributed to synergistic effect from respective components (Cu_2O NPs and PZM) plus the SiO_2 spheres.

4. Conclusions

In summary, we developed a facile but effective method to fabricate cross-linked organic–inorganic polyphosphazene nanoshells via precipitation polymerization using SiO_2 as a template. Then, SiO_2@PZM@Cu nanospheres were synthesized by loading the Cu_2O NPs on the surface of SiO_2@PZM core-shell structures followed by chemical reduction. After cross-linking assembly and chemical reduction, the SiO_2 spheres were encapsulated by the PZM phase and uniform distributed the Cu_2O NPs. and its composition and structure was identified by FT-IR, XRD, XPS and EDS. The morphological characterization showed that, the resulting SiO_2@PZM@Cu composites exhibited that SiO_2 spheres were packaged by the PZM shells and uniform distributed Cu_2O NPs. Incorporation of 2 wt% SiO_2@PZM@Cu into EP led to the increase of the char yield and the decrease of DTG peak value. Moreover, the PHRR, THR, TSR, PSPR, and MAHRE values for EP/SiO_2@PZM@Cu were obviously reduced. TG-FTIR results presented that the amount of toxic CO and other volatile products from the EP decomposition significantly suppressed after incorporating the SiO_2@PZM@Cu hybrids, implying a reduced toxicity. A flame-retardant mechanism was suggested based on the analyses of char residue and pyrolysis fragments. The significant enhancement of flame retardancy and toxic effluents elimination was primarily due to the synergistic action between the catalytic effect of SiO_2 and Cu_2O NPs and intumescent effect of PZM.

References

[1] N.L. Morozowich, J.L. Nichol, H.R. Allcock, Investigation of apatite mineralization on antioxidant polyphosphazenes for bone tissue engineering, Chem. Mater. 24 (2012) 3500-3509.

[2] Y. Hu, L. Meng, L. Niu, Q. Lu, Facile synthesis of superparamagnetic Fe3O4@ polyphosphazene@ Au shells for magnetic resonance imaging and photothermal therapy, ACS Appl. Mater. Inter. 5 (2013) 4586-4591.

[3] Z. Tian, A. Hess, C.R. Fellin, H. Nulwala, H.R. Allcock, Phosphazene High Polymers and Models with Cyclic Aliphatic Side Groups: New Structure–Property Relationships, Macromolecules 48 (2015) 4301-4311.

[4] I. Teasdale, O. Brüggemann, Polyphosphazenes: multifunctional, biodegradable vehicles for drug and gene delivery, Polymers 5 (2013) 161-187.

[5] D. He, S.Y. Cho, D.W. Kim, C. Lee, Y. Kang, Enhanced ionic conductivity of semi-IPN solid polymer electrolytes based on star-shaped oligo (ethyleneoxy) cyclotriphosphazenes, Macromolecules 45 (2012) 7931-7938.

[6] T. Modzelewski, H.R. Allcock, An Unusual Polymer Architecture for the Generation of Elastomeric Properties in Fluorinated Polyphosphazenes, Macromolecules 47 (2014) 6776-6782.

[7] T. Mayer-Gall, D. Knittel, J.S. Gutmann, K. Opwis, Permanent flame retardant finishing of textiles by allyl-functionalized polyphosphazenes, ACS Appl. Mater. Inter. 7 (2015) 9349-9363.

[8] L. Zhu, Y. Zhu, Y. Pan, Y. Huang, X. Huang, X. Tang, Fully Crosslinked Poly [cyclotriphosphazene-co-(4, 4′-sulfonyldiphenol)] Microspheres via Precipitation Polymerization and Their Superior Thermal Properties, Macromol. React. Eng. 1 (2007) 45-52.

[9] H. Liu, X. Wang, D. Wu, Novel cyclotriphosphazene-based epoxy compound and its application in halogen-free epoxy thermosetting systems: Synthesis, curing behaviors, and flame retardancy, Polym. Degrad. Stabil. 103 (2014) 96-112.

[10] W. Jin, L. Yuan, G. Liang, A. Gu, Multifunctional cyclotriphosphazene/

hexagonal boron nitride hybrids and their flame retarding bismaleimide resins with high thermal conductivity and thermal stability, ACS Appl. Mater. Inter. 6 (2014) 14931-14944.

[11] J. Fu, X. Huang, Y. Huang, J. Zhang, X. Tang, One-pot noncovalent method to functionalize multi-walled carbon nanotubes using cyclomatrix-type polyphosphazenes, Chem. Commun. (2009) 1049-1051.

[12] J. Fu, Q. Xu, J. Chen, Z. Chen, X. Huang, X. Tang, Controlled fabrication of uniform hollow core porous shell carbon spheres by the pyrolysis of core/shell polystyrene/cross-linked polyphosphazene composites, Chem. Commun. 46 (2010) 6563-6565.

[13] L. Zhu, Y. Xu, W. Yuan, J. Xi, X. Huang, X. Tang, S. Zheng, One-Pot Synthesis of Poly (cyclotriphosphazene-co-4, 4′-sulfonyldiphenol) Nanotubes via an In Situ Template Approach, Adv. Mater. 18 (2006) 2997-3000.

[14] M. Wang, J. Fu, D. Huang, C. Zhang, Q. Xu, Silver nanoparticles-decorated polyphosphazene nanotubes: synthesis and applications, Nanoscale 5 (2013) 7913-7919.

[15] X. Gu, X. Huang, H. Wei, X. Tang, Synthesis of novel epoxy-group modified phosphazene-containing nanotube and its reinforcing effect in epoxy resin, Eur. Polym. J. 47 (2011) 903-910.

[16] W. Liu, Y. Zheng, J. Li, L. Liu, X. Huang, J. Zhang, X. Kang, X. Tang, Novel polyurethane networks based on hybrid inorganic/organic phosphazene‐containing nanotubes with surface active hydroxyl groups, Polym. Adv. Technol. 23 (2012) 1-7.

[17] K. Chen, X. Huang, X. Tang, L. Zhu, Study on the Organic–Inorganic Hybrid Polyphosphazene Nanotube as a Flame Retardant for Polypropylene, J. Macromol. Sci. B 51 (2012) 269-274.

[18] C.E. Stere, W. Adress, R. Burch, S. Chansai, A. Goguet, W.G. Graham, F. De Rosa, V. Palma, C. Hardacre, Ambient Temperature Hydrocarbon Selective Catalytic Reduction of NO_x Using Atmospheric Pressure Nonthermal Plasma Activation of a Ag/Al_2O_3 Catalyst, ACS Catal. 4 (2014) 666-673.

[19] Y.-G. Wang, Y. Yoon, V.-A. Glezakou, J. Li, R. Rousseau, The role of reducible

oxide–metal cluster charge transfer in catalytic processes: new insights on the catalytic mechanism of CO oxidation on Au/TiO_2 from ab initio molecular dynamics, J. Am. Chem. Soc. 135 (2013) 10673-10683.

[20] J.R. Manders, S.W. Tsang, M.J. Hartel, T.H. Lai, S. Chen, C.M. Amb, J.R. Reynolds, F. So, Solution-Processed Nickel Oxide Hole Transport Layers in High Efficiency Polymer Photovoltaic Cells, Adv. Funct. Mater. 23 (2013) 2993-3001.

[21] Q. He, T. Yuan, S. Wei, Z. Guo, Catalytic and synergistic effects on thermal stability and combustion behavior of polypropylene: influence of maleic anhydride grafted polypropylene stabilized cobalt nanoparticles, J. Mater. Chem. A 1 (2013) 13064-13075.

[22] P.D. Tran, S.K. Batabyal, S.S. Pramana, J. Barber, L.H. Wong, S.C.J. Loo, A cuprous oxide-reduced graphene oxide (Cu_2O-rGO) composite photocatalyst for hydrogen generation: employing rGO as an electron acceptor to enhance the photocatalytic activity and stability of Cu_2O, Nanoscale 4 (2012) 3875-3878.

[23] L.Y. Isseroff, E.A. Carter, Electronic structure of pure and doped cuprous oxide with copper vacancies: suppression of trap states, Chem. Mater. 25 (2013) 253-265.

[24] Q. Yang, M. Long, L. Tan, Y. Zhang, J. Ouyang, P. Liu, A. Tang, Helical TiO_2 nanotube arrays modified by Cu-Cu_2O with ultrahigh sensitivity for the nonenzymatic electro-oxidation of glucose, ACS Appl. Mater. Inter. 7 (2015) 12719-12730.

[25] L. Liu, W. Yang, Q. Li, S. Gao, J.K. Shang, Synthesis of Cu_2O nanospheres decorated with TiO_2 nanoislands, their enhanced photoactivity and stability under visible light illumination, and their post-illumination catalytic memory, ACS Appl. Mater. Inter. 6 (2014) 5629-5639.

[26] T.-J. Huang, D.-H. Tsai, CO oxidation behavior of copper and copper oxides, Catal. Lett. 87 (2003) 173-178.

[27] B. White, M. Yin, A. Hall, D. Le, S. Stolbov, T. Rahman, N. Turro, S. O'Brien, Complete CO oxidation over Cu_2O nanoparticles supported on silica gel, Nano lett. 6 (2006) 2095-2098.

[28] S.-D. Jiang, L. Song, W.-R. Zeng, Z.-Q. Huang, J. Zhan, A.A. Stec, T.R. Hull, Y. Hu, W.-Z. Hu, Self-Assembly Fabrication of Hollow Mesoporous Silica@Co–Al

Layered Double Hydroxide@ Graphene and Application in Toxic Effluents Elimination, ACS Appl. Mater. Inter. 7 (2015) 8506-8514.

[29] W. Xu, L. Liu, B. Zhang, Y. Hu, B. Xu, Effect of Molybdenum Trioxide-Loaded Graphene and Cuprous Oxide-Loaded Graphene on Flame Retardancy and Smoke Suppression of Polyurethane Elastomer, Ind. Eng. Chem. Res. (2016).

[30] S.-D. Jiang, Z.-M. Bai, G. Tang, L. Song, A.A. Stec, T.R. Hull, J. Zhan, Y. Hu, Fabrication of Ce-doped MnO_2 decorated graphene sheets for fire safety applications of epoxy composites: flame retardancy, smoke suppression and mechanism, J. Mater. Chem. A 2 (2014) 17341-17351.

[31] C.W. Li, M.W. Kanan, CO_2 reduction at low overpotential on Cu electrodes resulting from the reduction of thick Cu_2O films, J. Am. Chem. Soc. 134 (2012) 7231-7234.

[32] J. Jiang, Y. Cheng, Y. Liu, Q. Wang, Y. He, B. Wang, Intergrowth charring for flame-retardant glass fabric-reinforced epoxy resin composites, J. Mater. Chem. A 3 (2015) 4284-4290.

[33] H. Gu, J. Guo, H. Wei, S. Guo, J. Liu, Y. Huang, M.A. Khan, X. Wang, D.P. Young, S. Wei, Z. Guo, Strengthened magnetoresistive epoxy nanocomposite papers derived from synergistic nanomagnetite-carbon nanofiber nanohybrids, Adv. Mater. 27 (2015) 6277-6282.

[34] J. Guo, J. Long, D. Ding, Q. Wang, Y. Shan, A. Umar, X. Zhang, B. L. Weeks, S. Wei, Z. Guo, Significantly enhanced mechanical and electrical properties of epoxy nanocomposites reinforced with low loading of polyaniline nanoparticles, RSC Adv. 6 (2016) 21187-21192.

[35] K. Zhou, J. Liu, Y. Shi, S. Jiang, D. Wang, Y. Hu, Z. Gui, MoS_2 nanolayers grown on carbon nanotubes: an advanced reinforcement for epoxy composites, ACS Appl. Mater. Inter. 7 (2015) 6070-6081.

[36] S.-H. Liao, P.-L. Liu, M.-C. Hsiao, C.-C. Teng, C.-A. Wang, M.-D. Ger, C.-L. Chiang, One-step reduction and functionalization of graphene oxide with phosphorus-based compound to produce flame-retardant epoxy nanocomposite, Ind. Eng. Chem. Res. 51 (2012) 4573-4581.

[37] H. Gu, C. Ma, J. Gu, J. Guo, X. Yan, J. Huang, Q. Zhang, Z. Guo, An overview of multifunctional epoxy nanocomposites, J. Mater. Chem. C. 4 (2016) 5890-5906.

[38] B. Yu, W. Xing, W. Guo, S. Qiu, X. Wang, S. Lo, Y. Hu, Thermal exfoliation of hexagonal boron nitride for effective enhancements on thermal stability, flame retardancy and smoke suppression of epoxy resin nanocomposites via sol–gel process, J. Mater. Chem. A 4 (2016) 7330-7340.

[39] X. Wang, S. Zhou, W. Xing, B. Yu, X. Feng, L. Song, Y. Hu, Self-assembly of Ni–Fe layered double hydroxide/graphene hybrids for reducing fire hazard in epoxy composites, J. Mater. Chem. A 1 (2013) 4383-4390.

[40] S. Wang, F. Xin, Y. Chen, L. Qian, Y. Chen, Phosphorus-nitrogen containing polymer wrapped carbon nanotubes and their flame-retardant effect on epoxy resin, Polym. Degrad. Stabil. 129 (2016) 133-141.

[41] H. Gu, J. Guo, H. Wei, X. Yan, D. Ding, X. Zhang, Q. He, S. Tadakamalla, X. Wang, T.C. Ho, Transparent anhydride-cured epoxy nanocomposites reinforced with polyaniline stabilized nanosilica, J. Mater. Chem. C 3 (2015) 8152-8165.

[42] X. Qian, L. Song, B. Yu, B. Wang, B. Yuan, Y. Shi, Y. Hu, R.K. Yuen, Novel organic–inorganic flame retardants containing exfoliated graphene: preparation and their performance on the flame retardancy of epoxy resins, J. Mater. Chem. A 1 (2013) 6822-6830.

[43] S.-D. Jiang, Z.-M. Bai, G. Tang, L. Song, A.A. Stec, T.R. Hull, Y. Hu, W.-Z. Hu, Synthesis of Mesoporous Silica@Co–Al Layered Double Hydroxide Spheres: Layer-by-Layer Method and Their Effects on the Flame Retardancy of Epoxy Resins, ACS Appl. Mater. Inter. 6 (2014) 14076-14086.

[44] H. Gu, J. Guo, Q. He, S. Tadakamalla, X. Zhang, X. Yan, Y. Huang, H.A. Colorado, S. Wei, Z. Guo, Flame-retardant epoxy resin nanocomposites reinforced with polyaniline-stabilized silica nanoparticles, Ind. Eng. Chem. Res. 52 (2013) 7718-7728.

[45] D. Wang, L. Song, K. Zhou, X. Yu, Y. Hu, J. Wang, Anomalous nano-barrier effects of ultrathin molybdenum disulfide nanosheets for improving the flame retardance of polymer nanocomposites, J. Mater. Chem. A 3 (2015) 14307-14317.

[46] X. Wang, L. Song, H. Yang, W. Xing, B. Kandola, Y. Hu, Simultaneous reduction and surface functionalization of graphene oxide with POSS for reducing fire hazards in epoxy composites, J. Mater. Chem. 22 (2012) 22037-22043.

[47] X. Zhang, O. Alloul, Q. He, J. Zhu, M.J. Verde, Y. Li, S. Wei, Z. Guo, Strengthened magnetic epoxy nanocomposites with protruding nanoparticles on the graphene nanosheets, Polymer 54 (2013) 3594-3604.

[48] H. Yu, J. Liu, X. Wen, Z. Jiang, Y. Wang, L. Wang, J. Zheng, S. Fu, T. Tang, Charing polymer wrapped carbon nanotubes for simultaneously improving the flame retardancy and mechanical properties of epoxy resin, Polymer 52 (2011) 4891-4898.

[49] Y. Zuo, Y. Zhang, Y. Fu, Catalytic conversion of cellulose into levulinic acid by a sulfonated chloromethyl polystyrene solid acid catalyst, ChemCatChem 6 (2014) 753-757.

[50] J.B. Joo, I. Lee, M. Dahl, G.D. Moon, F. Zaera, Y. Yin, Controllable synthesis of mesoporous TiO_2 hollow shells: toward an efficient photocatalyst, Adv. Funct. Mater. 23 (2013) 4246-4254.

[51] J. Eiblmeier, M. Kellermeier, M. Deng, L. Kienle, J.M. Garcia Ruiz, W. Kunz, Bottom-Up Self-Assembly of Amorphous Core–Shell–Shell Nanoparticles and Biomimetic Crystal Forms in Inorganic Silica–Carbonate Systems, Chem. Mater. 25 (2013) 1842-1851.

[52] D. Cantillo, C.O. Kappe, Immobilized Transition Metals as Catalysts for Cross-Couplings in Continuous Flow-A Critical Assessment of the Reaction Mechanism and Metal Leaching, ChemCatChem 6 (2014) 3286-3305.

[53] J.-B. Wu, X. Zhang, M. Ijäs, W.-P. Han, X.-F. Qiao, X.-L. Li, D.-S. Jiang, A.C. Ferrari, P.-H. Tan, Resonant Raman spectroscopy of twisted multilayer graphene, Nat. commun. 5 (2014).

[54] S. Qiu, W. Hu, B. Yu, B. Yuan, Y. Zhu, S. Jiang, B. Wang, L. Song, Y. Hu, Effect of Functionalized Graphene Oxide with Organophosphorus Oligomer on the Thermal and Mechanical Properties and Fire Safety of Polystyrene, Ind. Eng. Chem. Res. 54 (2015) 3309-3319.

[55] S.Y. Cho, H.R. Allcock, Novel highly fluorinated perfluorocyclobutane-based

phosphazene polymers for photonic applications, Chem. Mater. 19 (2007) 6338-6344.

[56] S. Mallakpour, M. Vahabi, The surface modification of CuO nanoparticles with a flame retardant coupling agent and their influence on the thermal stability of poly (amide-imide)/CuO nanocomposites, J. Compos. Mater. 50 (2016) 1971-1979.

[57] J.B. DeCoste, G.W. Peterson, Metal-organic frameworks for air purification of toxic chemicals, Chem. rev. 114 (2014) 5695-5727.

[58] S. Royer, D. Duprez, Catalytic oxidation of carbon monoxide over transition metal oxides, ChemCatChem 3 (2011) 24-65.

[59] B.-Z. Sun, X.-L. Xu, W.-K. Chen, L.-H. Dong, Theoretical insights into the reaction mechanisms of NO oxidation catalyzed by Cu_2O (111), Appl. Surf. Sci. 316 (2014) 416-423.

[60] M.-J. Chen, Y.-C. Lin, X.-N. Wang, L. Zhong, Q.-L. Li, Z.-G. Liu, Influence of Cuprous Oxide on Enhancing the Flame Retardancy and Smoke Suppression of Epoxy Resins Containing Microencapsulated Ammonium Polyphosphate, Ind. Eng. Chem. Res. (2015).

Author information

Corresponding Authors

*Yuan Hu. Fax/Tel: +86-551-63601664. E-mail: yuanhu@ustc.edu.cn.

*Weiyi Xing. Fax/Tel: +86-551-63602353. E-mail: xingwy@ustc.edu.cn.

Acknowledgements

The work was financially supported by the National Natural Science Foundation of China (No. 21374111), the Fundamental Research Funds for the Central Universities (WK2320000032), the Anhui Provincial Natural Science Foundation (1608085QE99), and the grants from the Research Grant Council of the Hong Kong Special Administrative Region, China (Project number CityU 11301015 and T32-101/15-R, respectively).

Scheme 1. Synthetic route of SiO_2@PZM@Cu.

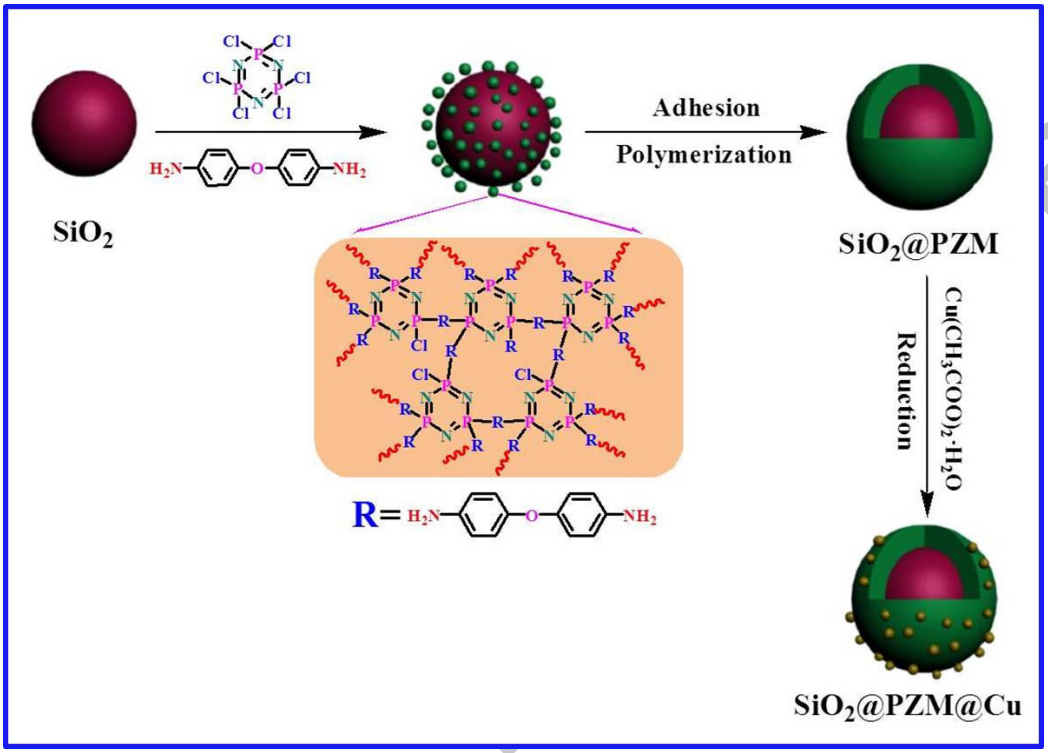

Fig. 1. TEM images of SiO_2 (A) and SiO_2@PZM (B, C); SEM images of SiO_2 (D) and SiO_2@PZM (E).

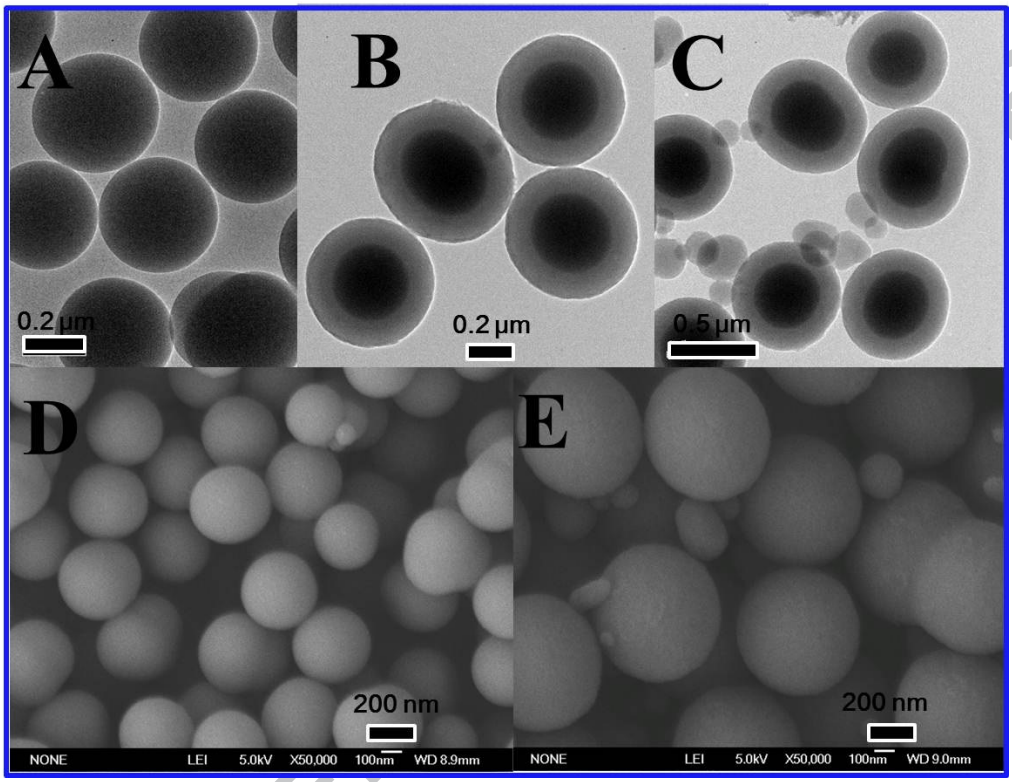

Fig. 2. TEM images of SiO_2@PZM@Cu (A, B, C); SEM images of SiO_2@PZM@Cu (D, E); and EDX spectrum (F) of SiO_2@PZM@Cu.

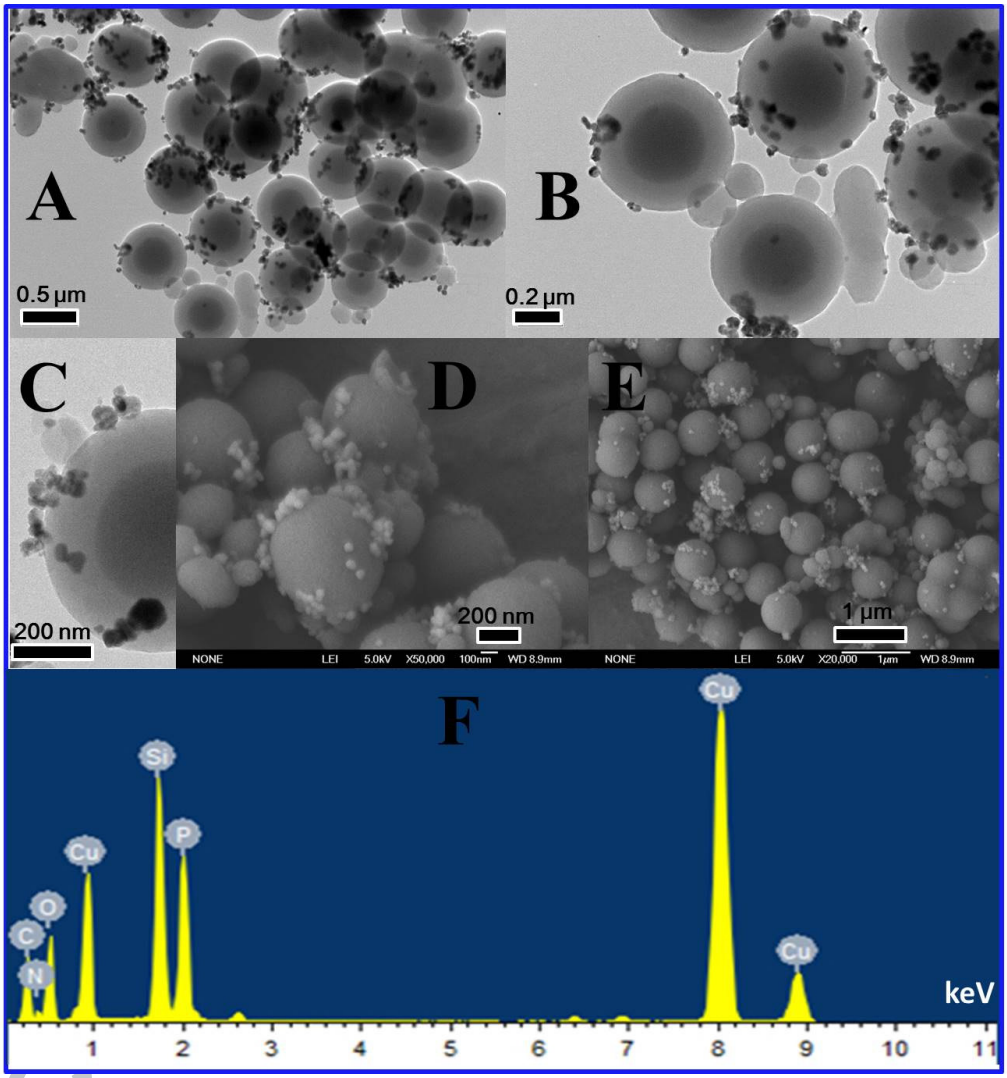

Fig. 3. (A) FT-IR spectra; (B) Wide-angle XRD patterns; (C) XPS survey spectra; (D) TGA curves of SiO_2, SiO_2@PZM and SiO_2@PZM@Cu.

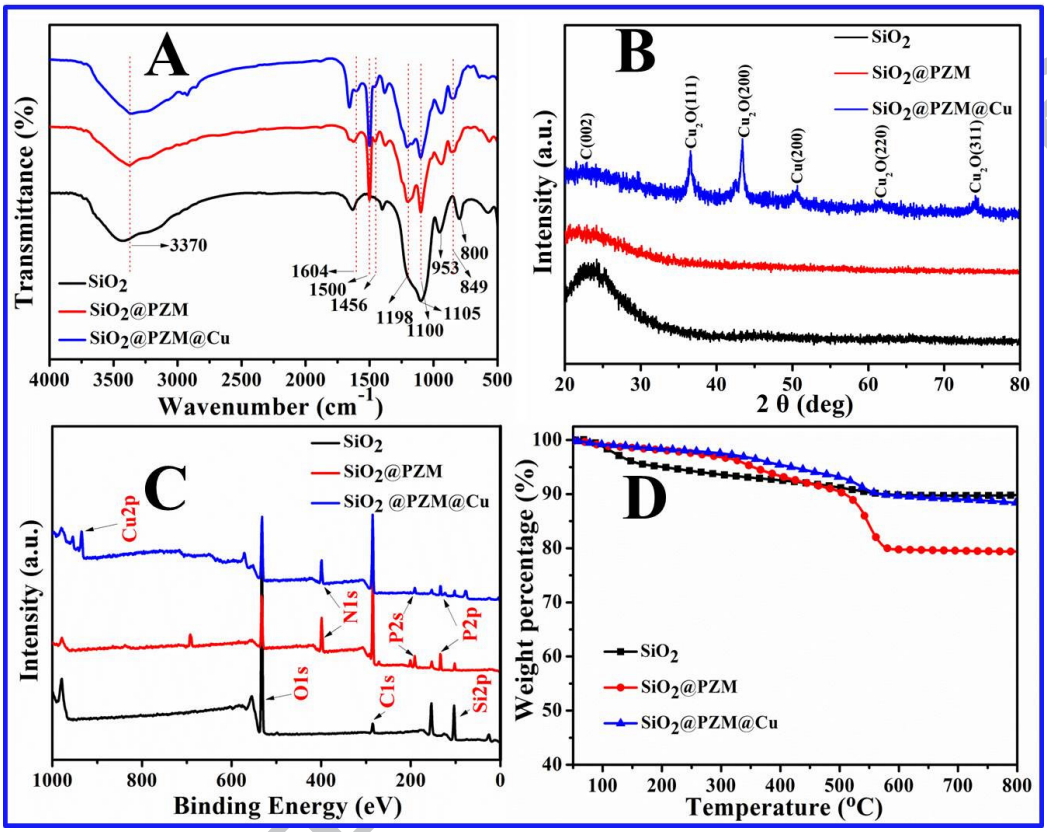

Fig. 4. (A) TGA curves of pure EP and its nanocomposites and (B) DTA curves of pure EP and its nanocomposites in nitrogen.

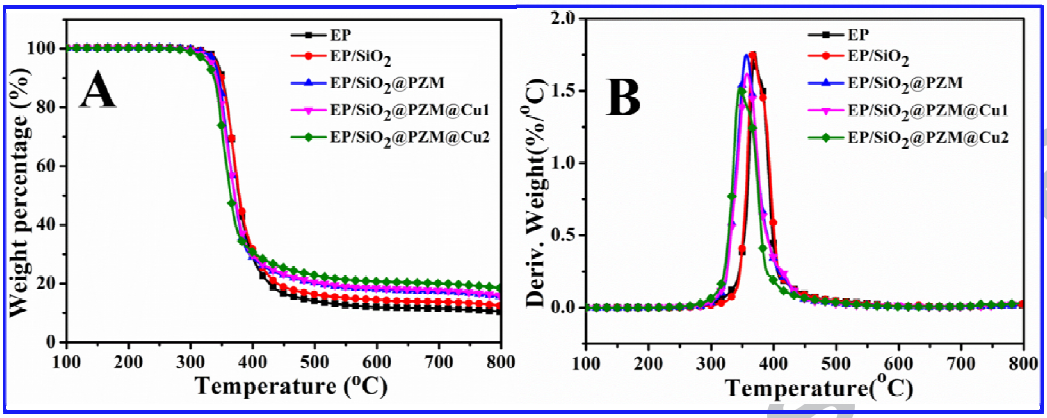

Fig. 5. SEM images of the fracture surfaces of (A) pure EP; (B) EP/SiO_2; (C) EP/SiO_2@PZM; (D) EP/SiO_2@PZM@Cu1 and (E,F) EP/SiO_2@PZM@Cu2.

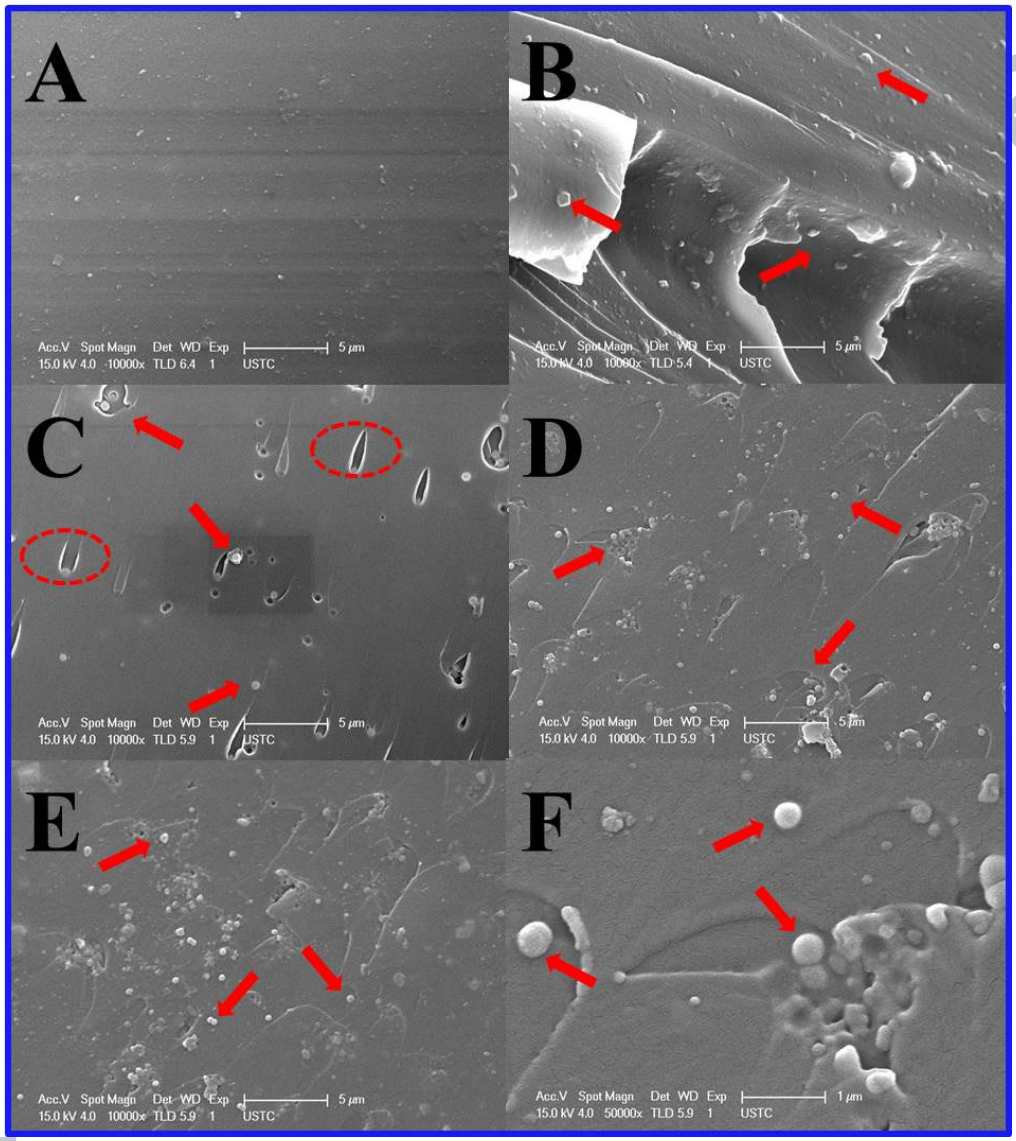

Fig. 6. HRR (A) and THR (B) vs. time curves of EP and its nanocomposites obtained from cone calorimeter.

.

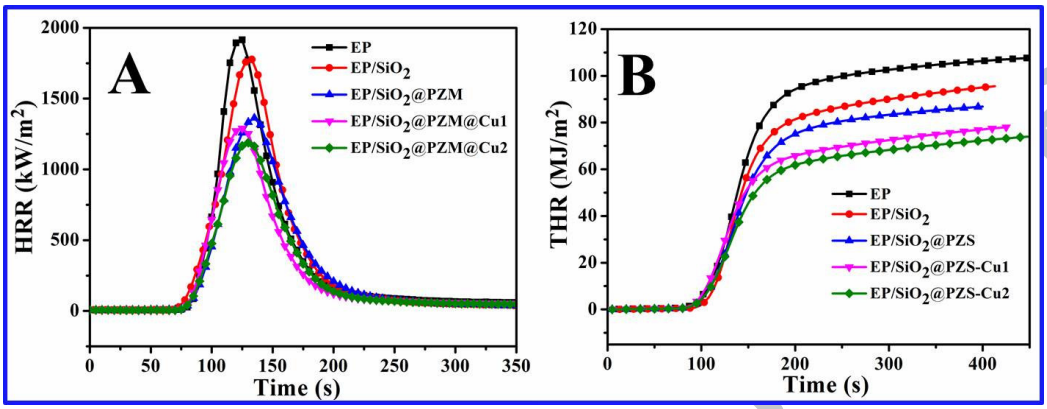

Fig. 7. SPR (A) and TSR (B) vs. time curves of EP and its nanocomposites obtained from cone calorimeter.

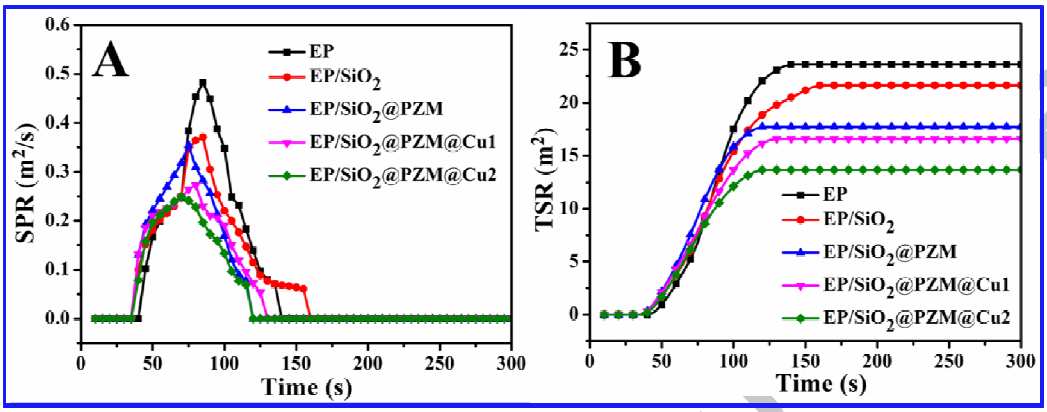

Fig. 8. (A) Three-dimensional (3D) TG-FTIR spectra of gasified pyrolysis products for pure EP and EP/SiO_2@PZM@Cu1. (B) FTIR spectra of gasified pyrolysis products for pure EP and EP/SiO_2@PZM@Cu1 at the maximum evolution rate.

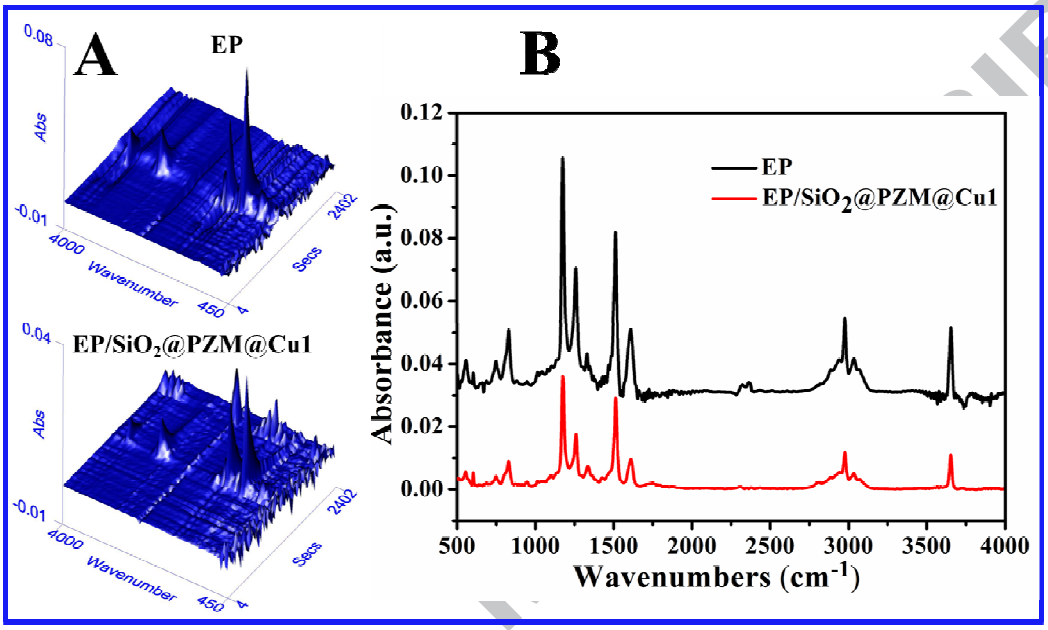

Fig. 9. FTIR spectra of the pyrolysis products for EP (A) and EP/SiO_2@PZM@Cu1 (B) at different temperatures.

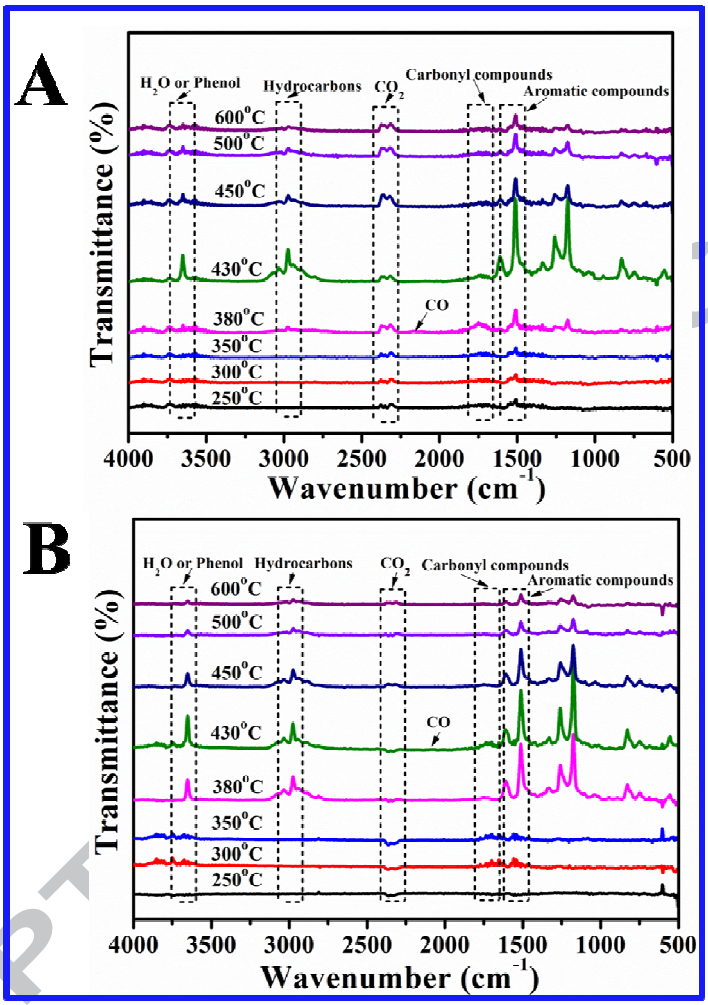

Fig. 10. Absorbance of pyrolysis products for EP and its nanocomposites vs. time: (A) total pyrolysis products, (B) hydrocarbons, (C) CO, (D) CO_2, (E) carbonyl and (F) aromatic compounds.

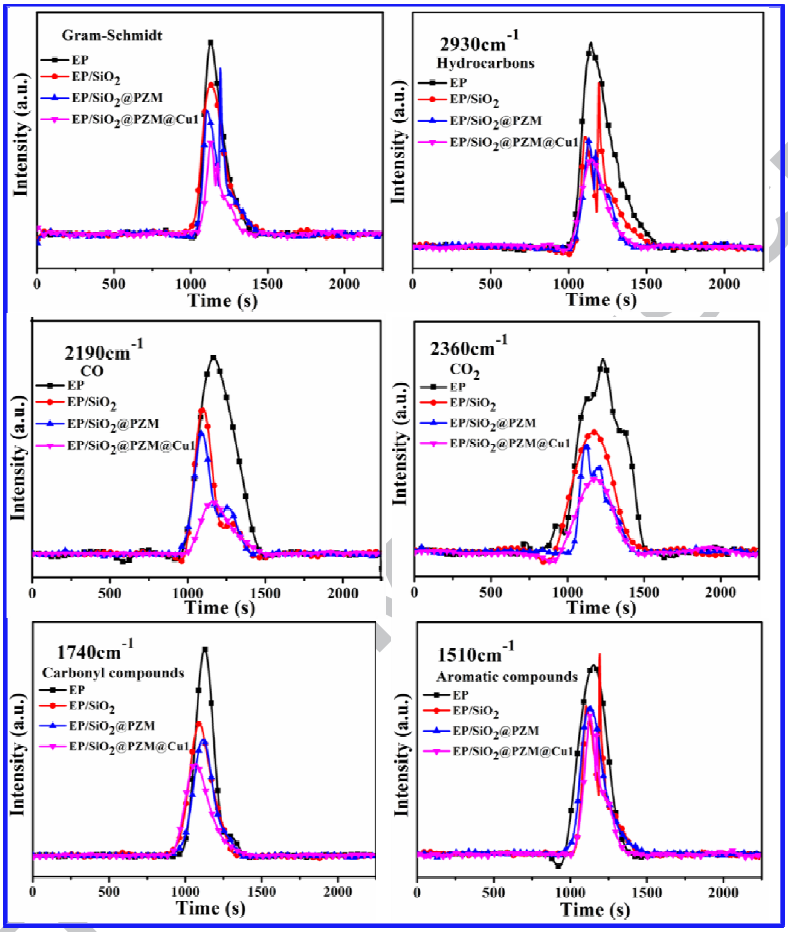

Fig. 11. Digital photos (A, B), Raman spectra (C, D) and SEM images (E, F) of the char residues from EP and EP/SiO_2@PZM@Cu1.

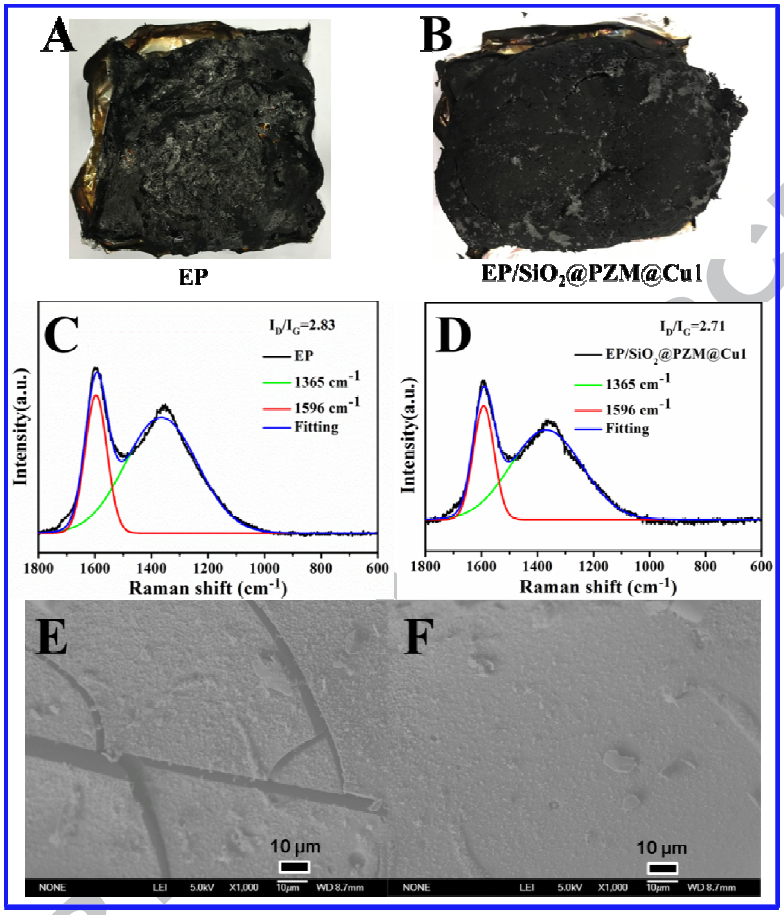

Fig. 12 FTIR spectra (A) and XRD patterns (B) of the char residues for EP and its nanocomposites after cone calorimeter tests.

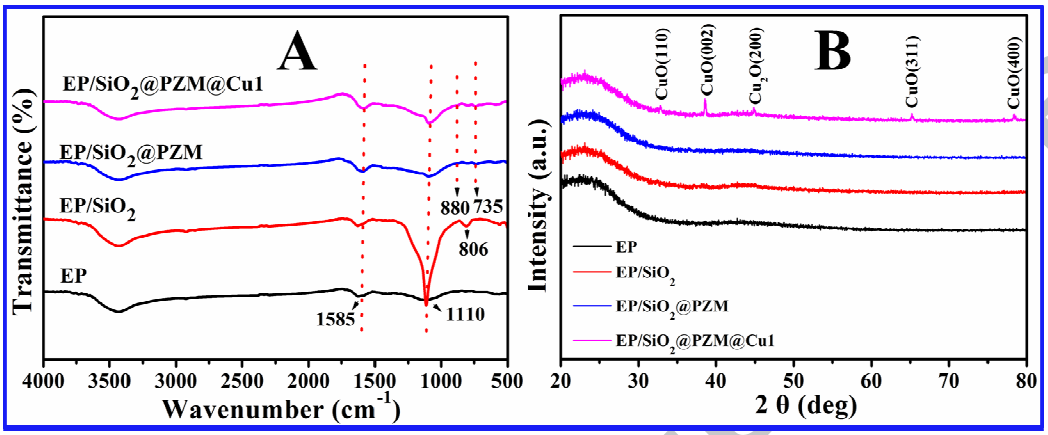

Scheme 2. Schematic illustration of mechanism for flame retardancy and toxic effluents elimination of SiO_2@PZM@Cu in flaming EP composites.

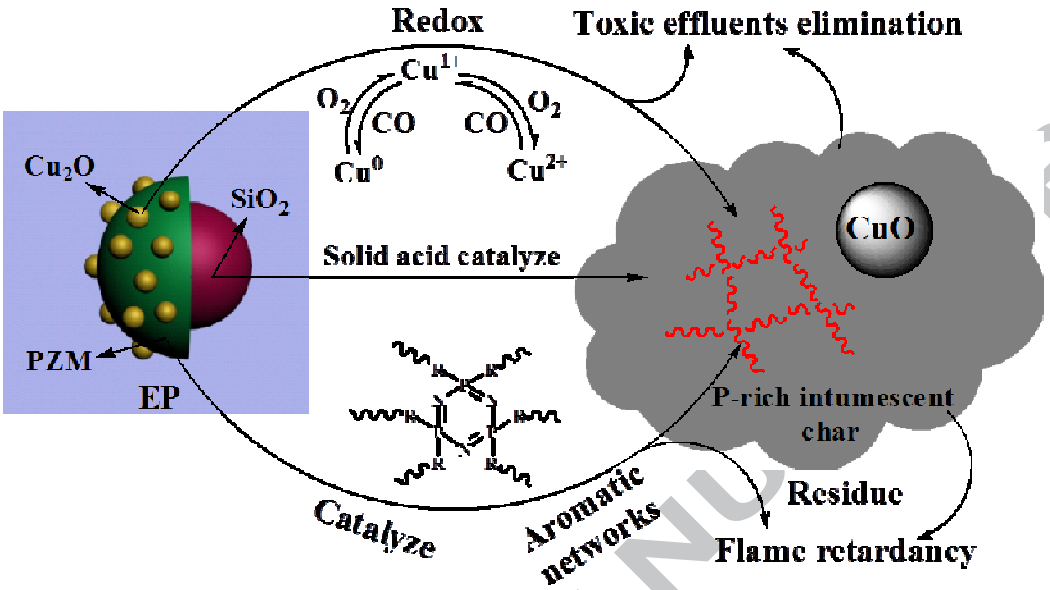

Table 1 Combustion property of EP nanocomposites reported in literature

Literature	PHRR (kW m^{-2} or W g^{-1})	THR (MJ m^{-2} or kJ m^{-2})	Reference
7.0 wt% u-silica	~(−)25%	~(−)8%	[44]
2.0 wt% MoS_2	~(−)43%	~(−)14%	[45]
3.0 wt% h-BN	~(−)53 %	~(−)32%	[38]
2.0 wt% OapPOSS-rGO	~(−)38%	~(−)36%	[46]
5.0 wt% Gr/Fe@Fe_2O_3	~(−)15%	~(−)20%	[47]
3.0 wt% CNT-PR	~(−)33%	Not reported	[48]

Table 2. TGA data for EP and its nanocomposites in nitrogen

Sample	$T_{-5\%}$ (°C)	$T_{-50\%}$ (°C)	T_{max} (°C)	Residue at 800 °C (wt%)
EP	**343.5**	**377.4**	**368.9**	**10.4**
EP/SiO_2	**341.9**	**378.5**	**367.4**	**12.4**
EP/SiO_2@PZM	**338.9**	**370.7**	**356.2**	**15.7**
EP/SiO_2@PZM@Cu1	**333.5**	**371.0**	**357.4**	**16.0**
EP/SiO_2@PZM@Cu2	**327.6**	**364.1**	**346.2**	**18.5**

Table 3. Cone calorimeter data of EP and its nanocomposites

Sample	T_{PHRR} (s)	PHRR (kW/m^2)	THR (MJ/m^2)	PSPR (m^2/s)	TSR (m^2)	MARHE (kW/m^2)
EP	**125**	**1915.3**	**107.6**	**0.48**	**23.6**	**667.4**
EP/SiO_2	**133**	**1776.9**	**95.6**	**0.37**	**21.6**	**614.8**
EP/SiO_2@PZM	**135**	**1363.4**	**86.8**	**0.35**	**17.7**	**564.2**
EP/SiO_2@PZM@Cu1	**125**	**1289.3**	**78.0**	**0.27**	**16.6**	**494.3**
EP/SiO_2@PZM@Cu2	**130**	**1188.8**	**73.9**	**0.25**	**13.7**	**479.9**

Highlights

1. A novel 3D nanostructure was prepared via a facile but effective method.
2. EP/SiO_2@PZM@Cu showed significant decrease in PHRR, THR and the amount of CO.
3. The improvements attributed to synergistic catalytic effect.
4. Cu_2O played a role in conversion of CO to CO_2 through a redox cycle.